CMS Physics Analysis Summary

Search for beyond the standard model physics in events with two leptons of the same sign, missing transverse momentum, and jets in proton-proton collisions at $\sqrt{s} = 13$ TeV

The CMS Collaboration

Abstract

A data sample of events from proton-proton collisions with two isolated same-sign leptons, missing transverse momentum, and jets is studied in a search for signatures of new physics phenomena by the CMS Collaboration at the LHC. The integrated luminosity of the data set is 35.9 fb^{-1} and the center-of-mass energy of the collisions is 13 TeV. The properties of the events are well described by the expectations from the standard model processes. Exclusion limits at 95% confidence level are set on the pair production of gluinos, squarks, and same-sign top quarks, as well as top quark associated production of a heavy scalar or pseudoscalar boson decaying to top quarks, and on the standard model production of events with four top quarks. Additionally, model-independent limits in several topological regions are provided, allowing for further interpretations of the results.

1 Introduction

Final states with two leptons of the same charge, same-sign (SS) dileptons, are rarely produced by standard model (SM) processes in proton-proton collisions. Because the SM rates of SS dileptons are low, studies of these final states provide excellent opportunities to search for manifestations of physics beyond the standard model (BSM). Over the last decades, a large number of new physics mechanisms have been proposed to overcome the known shortcomings of the SM. Many of these can give rise to potentially large contributions to the SS dilepton signature, e.g., the production of supersymmetric (SUSY) particles [1, 2], SS top quarks [3, 4], sgluons [5, 6], heavy scalar bosons of extended Higgs sectors [7, 8], Majorana neutrinos [9], and vector-like quarks [10].

In the SUSY framework [11–20], the SS final state can appear in R-parity conserving models through gluino or squark pair production, when the decay of each of the pair-produced particles yields one or more W bosons. For example, a pair of gluinos (which are Majorana particles) can give rise to SS charginos and up to four top quarks, yielding signatures with up to four W bosons, as well as jets, b quark jets, and large missing transverse momentum (E_T^{miss}). Similar signatures can also result from the pair production of bottom squarks, subsequently decaying to charginos and top quarks.

While R-parity conserving SUSY models often lead to signatures with large E_T^{miss}, it is also interesting to study final states without large E_T^{miss} beyond that produced by the neutrinos from leptonic W decays. New physics scenarios can lead to the production of SS top quark pairs. Production of multiple top quarks can also lead to this signature, and can be realized in both the SM and BSM scenarios, such as the associated production of a heavy (pseudo)scalar, which subsequently decays to a pair of top quarks. Such a scenario is realized, for example, in Type II two Higgs doublet models (2HDM) where associated production with a single top quark or $t\bar{t}$ pair can provide a promising window to probe these heavy (pseudo)scalar bosons [21–23].

In addition to the above-mentioned interpretations, model-independent (MI) results are also provided in several kinematic regions, to allow further interpretations of the results. The MI results are given as a function of hadronic activity and of E_T^{miss}, as well as in a set of inclusive regions with different topologies. The full analysis results are also summarized in a smaller set of exclusive regions to be used in combination with the background correlation matrix to facilitate reinterpretations of the results, as discussed in Section 7.

This Physics Analysis Summary extends the search for new physics presented in Ref. [24]. We consider final states with either two muons, two electrons, or one muon and one electron, all of the same charge, two or more hadronic jets, and moderate E_T^{miss}. Compared to searches with zero or one lepton, this final state provides enhanced sensitivity to low-momentum leptons and SUSY models with compressed mass spectrum. The results are based on an integrated luminosity corresponding to 35.9 fb^{-1} of $\sqrt{s}$ = 13 TeV proton-proton (pp) collisions collected with the CMS detector at the CERN LHC. Previous LHC searches in the SS dilepton channel have been performed by the ATLAS [25–27] and CMS [24, 28–32] Collaborations. With respect to Ref. [24], the event categorization is extended to take advantage of the increased integrated luminosity, the estimate of rare SM backgrounds is improved, the (pseudo)scalar boson interpretation is included for the first time, and further information is included to allow for new interpretations.

2 Background and signal simulation

The Monte Carlo (MC) simulations are used to estimate SM backgrounds and to evaluate the efficiency for new physics models. The MADGRAPH5_AMC@NLO 2.2.2 [33] and POWHEG v2 [34, 35] next-to-leading order (NLO) generators are used to simulate almost all SM backgrounds based on the NNPDF3.0NLO [36] parton distribution functions (PDFs). New physics signal samples, as well as the same-sign WW process, are generated with MADGRAPH5_AMC@NLO at leading order (LO) precision, with up to two additional partons, using the NNPDF3.0LO [36] PDFs. Parton showering and hadronization, as well as the double parton scattering production of $W^{\pm}W^{\pm}$, are described using the PYTHIA 8.205 generator [37] with the CUETP8M1 tune [38, 39]. The GEANT4 package [40] is used to model the CMS detector response in background samples, while the CMS fast simulation package [41] is used for signal samples.

To improve on the MADGRAPH modeling of the multiplicity of additional jets from initial state radiation (ISR) , MADGRAPH $t\bar{t}$ MC events are reweighted based on the number of ISR jets (N_J^{ISR}) so as to make the jet multiplicity agree with that in data. The same reweighting procedure is applied to SUSY MC events. The reweighting factors vary between 0.92 and 0.51 for N_J^{ISR} between 1 and 6. We take one half of the deviation from unity as the systematic uncertainty in these reweighting factors

The new physics signal models probed by this search are shown in Figs. 1 and 2. In each of the simplified SUSY models [42, 43] of Fig. 1, only two or three new particles have masses sufficiently low to be produced on-shell, and the branching fraction for the decays shown are taken to be 100%. Gluino pair production models giving rise to signatures with up to four b quarks and up to four W bosons are shown in Figs. 1a–e. In these models, the gluino decays to the lightest squark, $\tilde{g} \rightarrow \tilde{q}q$, which can in turn decay to a quark of the same flavor, $\tilde{q} \rightarrow q\tilde{\chi}_1^0$, or of a different flavor, $\tilde{q} \rightarrow q'\tilde{\chi}^{\pm}$, with the chargino decay producing a W boson, $\tilde{\chi}^{\pm} \rightarrow W^{\pm}\tilde{\chi}_1^0$, and the $\tilde{\chi}_1^0$ (taken to be the lightest SUSY particle, or LSP) escaping detection. The first two scenarios considered in Figs. 1a and 1b include an off-shell third generation squark ($\tilde{t}$ or $\tilde{b}$) leading to the three-body decay of the gluino, $\tilde{g} \rightarrow t\bar{t}\tilde{\chi}_1^0$ (T1tttt) and $\tilde{g} \rightarrow \bar{t}b\tilde{\chi}^-$ (or T5ttbbWW), resulting in events with four W bosons and four b quarks. In the T5ttbbWW model, the mass splitting between chargino and neutralino is set to $m_{\tilde{\chi}^{\pm}} - m_{\tilde{\chi}_1^0} = 5\,\mathrm{GeV}$, so that two of the W bosons are produced off-shell and can give rise to low-p_{T} leptons. The next two models shown, Figures 1c,d, include an on-shell top squark with different mass splitting between the $\tilde{t}$ and the $\tilde{\chi}_1^0$, and consequently different decay modes: in the T5tttt model the mass splitting is equal to the top quark mass ($m_{\tilde{t}} - m_{\tilde{\chi}_1^0} = m_t$), favoring the $\tilde{t} \rightarrow t\tilde{\chi}_1^0$ decay, while in the T5ttcc model the mass splitting is only 20 GeV, favoring the flavor-changing $\tilde{t} \rightarrow c\tilde{\chi}_1^0$ decay.

In Figure 1e, the decay proceeds through a virtual light-flavor squark, leading to a three-body decay to $\tilde{g} \rightarrow qq'\tilde{\chi}^{\pm}$, resulting in a final state with two W bosons and four light flavor jets. The two W bosons can have the same charge, giving rise to SS dileptons. This model, T5qqqqWW, is studied as a function of the gluino and $\tilde{\chi}_1^0$ mass, with two different assumptions for the chargino mass: $m_{\tilde{\chi}^{\pm}} = 0.5(m_{\tilde{g}} - m_{\tilde{\chi}_1^0})$, producing mostly on-shell W bosons, and $m_{\tilde{\chi}^{\pm}} = m_{\tilde{\chi}_1^0} + 20\,\mathrm{GeV}$, producing off-shell W bosons. Finally, Fig. 1f shows a model of bottom squark production followed by the $\tilde{b} \rightarrow t\tilde{\chi}^{\pm}$ decay, resulting in two b quarks and four W bosons. This model, T6ttWW, is studied as a function of the $\tilde{b}$ and $\tilde{\chi}^{\pm}$ masses, keeping the $\tilde{\chi}_1^0$ mass at 50 GeV, resulting in two of the W bosons being produced off-shell when the $\tilde{\chi}^{\pm}$ and $\tilde{\chi}_1^0$ masses are close. The production cross sections for SUSY models are calculated at NLO plus next-to-leading logarithmic (NLL) accuracy [44–49].

The processes shown in Figure 2, $t\bar{t}H$, tHq and tWH, represent the top quark associated produc-

tion of a scalar (H) or pseudoscalar (A). The subsequent decay of H/A to a pair of top quarks gives rises to three or four top quark signatures. For the purpose of interpretation, we use LO cross sections for the production of a heavy Higgs boson in the context of the Type II 2HDM of Ref. [23]. The mass of the new particle is varied in the range [350, 550] GeV, where the lower mass boundary is chosen in such a way as to allow the decay of the (pseudo)scalar into on shell top quarks.
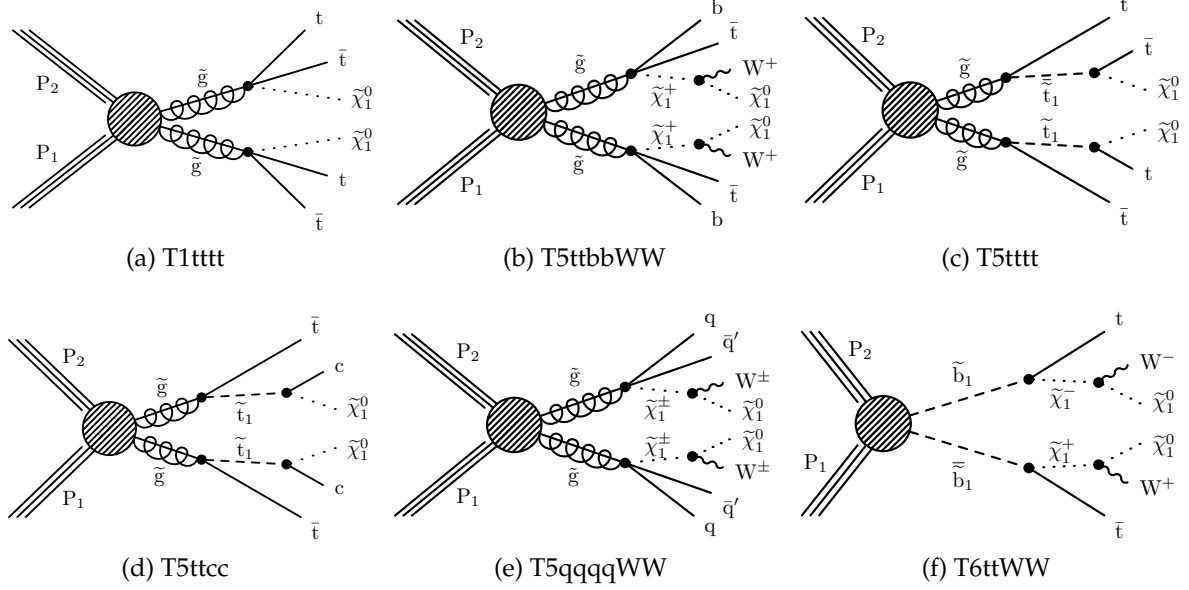

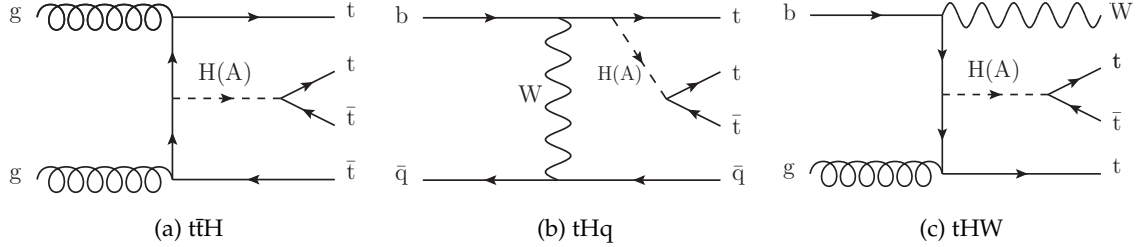Figure 1: Diagrams illustrating the simplified SUSY models considered in this analysis.

Figure 2: Diagrams for scalar (pseudoscalar) production in association with top quarks.

3   The CMS detector and event reconstruction

The central feature of the CMS detector is a superconducting solenoid of 6 m internal diameter, providing a magnetic field of 3.8 T. Within the solenoid volume are a silicon pixel and strip tracker, a lead tungstate crystal electromagnetic calorimeter (ECAL), and a brass and scintillator hadron calorimeter (HCAL), each composed of a barrel and two endcap sections. Forward calorimeters extend the pseudorapidity coverage provided by the barrel and endcap detectors. Muons are measured in gas-ionization detectors embedded in the steel flux-return yoke outside the solenoid. A more detailed description of the CMS detector, together with a definition of the coordinate system used and the relevant kinematic variables, can be found in Ref. [50].

Events of interest are selected using a two-tiered trigger system [51]. The first level (L1), composed of custom hardware processors, uses information from the calorimeters and muon de-

tectors to select events at a rate of around 100 kHz within a time interval of less than 4 μs. The second level, known as the high-level trigger (HLT), consists of a farm of processors running a version of the full event reconstruction software optimized for fast processing, and reduces the event rate to less than 1 kHz before data storage.

Events are processed using the particle-flow (PF) algorithm [52, 53], which reconstructs and identifies each individual particle with an optimized combination of information from the various elements of the CMS detector. The energy of photons is directly obtained from the ECAL measurement. The energy of electrons is determined from a combination of the electron momentum at the primary interaction vertex as determined by the tracker, the energy of the corresponding ECAL cluster, and the energy sum of all bremsstrahlung photons spatially compatible with originating from the electron track. The energy of muons is obtained from the curvature of the corresponding track, combining information from the silicon tracker and the muon system. The energy of charged hadrons is determined from a combination of their momentum measured in the tracker and the matching ECAL and HCAL energy deposits, corrected for zero suppression effects and for the response function of the calorimeters to hadronic showers. Finally, the energy of neutral hadrons is obtained from the corresponding corrected ECAL and HCAL energy.

Hadronic jets are clustered from neutral PF candidates and charged PF candidates associated to the primary vertex (PV), using the anti-k_t algorithm [54, 55] with a distance parameter $R = \sqrt{(\Delta\eta)^2 + (\Delta\phi)^2}$ of 0.4. Jet momentum is determined as the vectorial sum of all PF candidate momenta in the jet. An offset correction is applied to jet energies to take into account the contribution from additional proton-proton interactions (pileup) within the same or nearby bunch crossings. Jet energy corrections are derived from simulation, and are improved with in situ measurements of the energy balance in dijet and photon + jet events [56, 57]. Additional selection criteria are applied to each event to remove spurious jet-like features originating from isolated noise patterns in certain HCAL regions. The missing transverse momentum vector $\vec{p}_\mathrm{T}^{\,\mathrm{miss}}$ is defined as the projection on the plane perpendicular to the beams of the negative vector sum of the momenta of all reconstructed particles in an event. Its magnitude is referred to as $E_\mathrm{T}^{\mathrm{miss}}$. The scalar sum of the p_T of jets is referred to as H_T.

4   Event selection and search strategy

The event selection and the definition of the signal regions (SRs) follow closely the analysis strategy established in Ref. [24]. With respect to the previous search, the general strategy has remained unchanged. We target, in a generic way, new physics signatures that result in SS dileptons, hadronic activity and $E_\mathrm{T}^{\mathrm{miss}}$, by subdividing the event sample in several signal regions sensitive to a variety of new physics models. The number of signal regions has grown to take advantage of the larger integrated luminosity. Table 1 summarizes the basic kinematic requirements for jets and leptons (further details, including the lepton identification and isolation requirements, can be found in Ref. [24]).

Table 1: Kinematic requirements for leptons and jets.

Object	p_T	η
Electrons	$p_\mathrm{T} > 15\,\mathrm{GeV}$	$|\eta| < 2.5$
Muons	$p_\mathrm{T} > 10\,\mathrm{GeV}$	$|\eta| < 2.4$
Jets	$p_\mathrm{T} > 40\,\mathrm{GeV}$	$|\eta| < 2.4$
b-tagged jets	$p_\mathrm{T} > 25\,\mathrm{GeV}$	$|\eta| < 2.4$

Events are selected using triggers based on two sets of HLT algorithms, one simply requiring

two leptons, and one additionally requiring $H_T > 300\,\text{GeV}$. The H_T requirement allows to relax the lepton isolation and to set a p_T requirement of 8 GeV for both leptons, while in the pure dilepton trigger the leading and subleading leptons are required to have $p_T > 23\,(17)\,\text{GeV}$ and $p_T > 12\,(8)\,\text{GeV}$, respectively, for electrons (muons). Based on these trigger requirements, leptons are classified as "high" ($p_T > 25\,\text{GeV}$) and "low" momentum ($10 < p_T < 25\,\text{GeV}$), and three analysis regions are defined: high-high (HH), high-low (HL), and low-low (LL).

The lepton efficiency ranges between 45–70% (70–90%) for generated electrons (muons) with $p_T > 25\,\text{GeV}$, increasing as a function of p_T and converging to the maximum value for $p_T > 60\,\text{GeV}$. In the low momentum regime, $15 < p_T < 25\,\text{GeV}$ for electrons and $10 < p_T < 25\,\text{GeV}$ for muons, the efficiencies are 40% for electrons and 55% for muons. The b tagging working point chosen results in approximately a 70% efficiency for tagging a b quark jet and a smaller than 1% mistagging rate for light-quark and gluon jets in $t\bar{t}$ events. The efficiencies of the H_T and E_T^{miss} requirements are mostly determined by the jet energy and E_T^{miss} resolutions, which are discussed in Refs. [56–58].

The initial baseline selection used in this analysis requires at least one SS lepton pair with an invariant mass above 8 GeV, at least two jets, and $E_T^{\text{miss}} > 50\,\text{GeV}$. To reduce Drell–Yan backgrounds, events are rejected if an additional loose lepton forms an opposite-sign same-flavor pair with one of the two SS leptons, with an invariant mass less than 12 GeV or between 76 and 106 GeV. Events passing the baseline selection are then divided into signal regions to separate the different background processes and to maximize the sensitivity to signatures with different jet multiplicity (N_{jets}), flavor (N_b), visible and invisible energy (H_T and E_T^{miss}), and lepton momentum spectra (the HH/HL/LL categories mentioned above). The m_T^{min} variable, defined as the smallest of the transverse masses constructed between $\vec{p}_T^{\text{miss}}$ and each of the leptons, features a cutoff near the W boson mass for processes with only one prompt lepton, so it is used to create regions where the nonprompt lepton background is negligible. To further improve sensitivity, several regions are split according to the charge of the leptons (++ or --), taking advantage of the charge asymmetry of SM backgrounds with a single W boson produced in proton-proton collisions, such as $t\bar{t}W$ or WZ. Charge splitting is only applied to signal regions dominated by such backgrounds and with a sufficient predicted yield. In the HH and HL categories, events in the tail regions $H_T > 1125\,\text{GeV}$ or $E_T^{\text{miss}} > 300\,\text{GeV}$ are integrated in N_{jets}, N_b, and m_T^{min} in order to ensure a reasonable yield of events in these SRs. The exclusive SRs resulting from this classification are defined in Tables 2–4.

Table 2: Signal region definitions for the HH selection. Regions split by charge are indicated with (++) and (--).

N_b	m_T^{min} (GeV)	E_T^{miss} (GeV)	N_{jets}	$H_T < 300$ GeV	$H_T \in [300, 1125]$ GeV	$H_T \in [1125, 1300]$ GeV	$H_T \in [1300, 1600]$ GeV	$H_T > 1600$ GeV
0	< 120	50 − 200	2-4	SR1	SR2			
			≥5		SR4			
		200 − 300	2-4		SR5 (++) / SR6 (--)			
			≥5		SR7			
	> 120	50 − 200	2-4	SR3	SR8 (++) / SR9 (--)			
			≥5					
		200 − 300	2-4		SR10			
			≥5					
1	< 120	50 − 200	2-4	SR11	SR12			
			≥5		SR15 (++) / SR16 (--)			
		200 − 300	2-4		SR17 (++) / SR18 (--)			
			≥5		SR19			
	> 120	50 − 200	2-4	SR13 (++) / SR14 (--)	SR20 (++) / SR21 (--)	SR46 (++) / SR47 (--)	SR48 (++) / SR49 (--)	SR50 (++) / SR51 (--)
			≥5					
		200 − 300	2-4		SR22			
			≥5					
2	< 120	50 − 200	2-4	SR23	SR24			
			≥5		SR27 (++) / SR28 (--)			
		200 − 300	2-4		SR29 (++) / SR30 (--)			
			≥5		SR31			
	> 120	50 − 200	2-4	SR25 (++) / SR26 (--)	SR32 (++) / SR33 (--)			
			≥5					
		200 − 300	2-4		SR34			
			≥5					
≥3	< 120	50 − 200	≥2	SR35 (++) / SR36 (--)	SR37 (++) / SR38 (--)			
		200 − 300			SR39			
	> 120	50 − 300	≥2	SR40	SR41			
inclusive	inclusive	300 − 500	≥2	-	SR42 (++) / SR43 (--)			
		> 500		-	SR44 (++) / SR45 (--)			

Table 3: Signal region definitions for the HL selection. Regions split by charge are indicated with (++) and (--).

N_b	m_T^{min} (GeV)	E_T^{miss} (GeV)	N_{jets}	$H_T < 300$ GeV	$H_T \in [300, 1125]$ GeV	$H_T \in [1125, 1300]$ GeV	$H_T > 1300$ GeV
0	< 120	50 − 200	2-4	SR1	SR2		
			≥5		SR4		
		200 − 300	2-4	SR3	SR5 (++) / SR6 (--)		
			≥5		SR7		
1	< 120	50 − 200	2-4	SR8	SR9		
			≥5		SR12 (++) / SR13 (--)		
		200 − 300	2-4	SR10 (++) / SR11 (--)	SR14 (++) / SR15 (--)	SR38 (++) / SR39 (--)	SR40 (++) / SR41 (--)
			≥5		SR16 (++) / SR17 (--)		
2	< 120	50 − 200	2-4	SR18	SR19		
			≥5		SR22 (++) / SR23 (--)		
		200 − 300	2-4	SR20 (++) / SR21 (--)	SR24 (++) / SR25 (--)		
			≥5		SR26		
≥3	< 120	50 − 200	≥2	SR27 (++) / SR28 (--)	SR29 (++) / SR30 (--)		
		200 − 300			SR31		
inclusive	> 120	50 − 300	≥2	SR32	SR33		
inclusive	inclusive	300 − 500	≥2	-	SR34 (++) / SR35 (--)		
		> 500		-	SR36 (++) / SR37 (--)		

Table 4: Signal region definitions for the LL selection. All SRs in this category require $N_{jets} \geq 2$.

N_b	m_T^{min} (GeV)	H_T (GeV)	$E_T^{miss} \in [50, 200]$ GeV	$E_T^{miss} > 200$ GeV
0			SR1	SR2
1	< 120	> 300	SR3	SR4
2			SR5	SR6
≥ 3			SR7	
Inclusive	> 120		SR8	

5 Backgrounds

Standard model backgrounds arise from three sources: SM processes with prompt SS dileptons, mostly relevant in regions with tight kinematic selections; events with a nonprompt lepton, dominating the overall final state; and opposite-sign dilepton events with a charge-misidentified lepton, the smallest contribution.

Several categories of SM processes that result in the production of electroweak bosons can give rise to a SS dilepton final state: multiboson production of W, Z, H bosons, and prompt photons, as well as single-boson production in association with top quarks. Among these SM processes, the dominant ones are WZ, $t\bar{t}W$, and $t\bar{t}Z$ production, followed by the SS $W^{\pm}W^{\pm}$ process. The remaining SM processes are grouped into two categories, "Rare" (including ZZ, WWZ, WZZ, ZZZ, tWZ, tZq, as well as $t\bar{t}t\bar{t}$ and double parton scattering) and "X+γ" (including Wγ, Zγ, $t\bar{t}\gamma$, and tγ). The expected yields from these SM backgrounds are estimated from simulation, accounting for both theoretical and experimental uncertainties.

For the WZ and $t\bar{t}Z$ backgrounds, a three-lepton (3L) control region in data is used to scale the simulation, based on a template fit to the distribution of the number of b jets. The 3L control region requires at least two jets, $E_T^{\mathrm{miss}} > 30\,\mathrm{GeV}$, and three leptons, two of which must form an opposite-sign same-flavor pair with an invariant mass within 15 GeV of the Z boson mass. In the fit to data, the normalization and shapes of all the components are allowed to vary according to experimental and theoretical uncertainties. The scale factors obtained by the fit in the phase space of the 3L control region are 1.26 ± 0.09 for the WZ process, and 1.14 ± 0.30 for the $t\bar{t}Z$ process.

Nonprompt leptons are leptons from the decays of heavy- or light-flavor hadrons, hadrons misidentified as leptons, or electrons from conversions of photons in jets. The nonprompt lepton background, which is largest for regions with low m_T^{min} and low H_T, is estimated by the "tight-to-loose" method, which was employed in several previous versions of the analysis [28–32], and significantly improved in the latest version [24] to account for the kinematics and flavor of the mother parton of the nonprompt lepton. The tight-to-loose method uses two control regions enriched in nonprompt leptons, the application region and the measurement region. The former is based on each signal region selection, but requires that at least one lepton fails the nominal (tight) selection and passes the loose requirements, while the latter is a single-lepton region where electroweak processes (W and Z) are suppressed. For each lepton flavor (e or μ) and trigger (with or without isolation), a factor ϵ_{TL} – representing the probability for a nonprompt lepton that satisfies the loose selection to also satisfy the tight selection – is extracted from the measurement region as a function of lepton p_T^{corr} (defined below) and η. The ϵ_{TL} factors are then used to scale the yields observed in each application region to obtain the nonprompt predictions in each signal region. The p_T^{corr} parametrization, where p_T^{corr} is defined as the lepton p_T plus the energy in the isolation cone exceeding the isolation threshold value, is chosen because of its correlation with the mother parton p_T, improving the stability of ϵ_{TL} with respect to the sample kinematics. To improve the stability of ϵ_{TL} with respect to the mother parton flavor, the loose definition for electrons includes a relaxed selection chosen so that the ϵ_{TL} values are similar in nonprompt electrons from heavy- and light-flavor decays.

The prediction from the tight-to-loose method is cross-checked using an alternative method based on the same principle, similar to that described in Ref. [59]. In this cross-check, which aims to remove kinematic differences between measurement and application regions, the measurement region is obtained from SS dilepton events where one of the leptons fails the impact parameter requirement. With respect to the nominal method, the loose lepton definition is adapted to reduce the effect of the correlation between isolation and impact parameter. The

predictions of the two methods are found to be consistent in simulation and in data.

Charge misidentification of electrons is a small background that can arise from severe bremsstrahlung in the tracker material. Simulation studies on tightly selected leptons indicate that the muon charge misidentification probability is negligible, while for electrons it ranges between 10^{-5} and 10^{-3}. A low-E_T^{miss} control region, with $e^\pm e^\pm$ pairs in the Z boson mass window, is used to cross-check the MC prediction for the misidentification probability, both inclusively and – where the numbers of events in data allows it – as a function of electron p_T and η. The charge misidentification background is then estimated from an opposite-sign control region, defined for each SS SR, after scaling its yield by the charge misidentification probability.

6   Systematic uncertainties

Several sources of systematic uncertainty affect the predicted yields for signal and background processes, as summarized in Table 5. Experimental uncertainties are based on measurements in data of the trigger efficiency, lepton identification efficiency, b tagging efficiency, jet energy scale, and integrated luminosity, as well as on the inelastic cross section affecting the pileup rate. Theoretical uncertainties related to unknown higher-order effects are estimated by varying simultaneously the factorization and renormalization scales by a factor of two, while uncertainties in the PDFs are obtained using replicas of the NNPDF3.0 set [36].

Experimental and theoretical uncertainties affect both the overall yield ('normalization') and the relative population ('shape') across signal regions, and they are applied to all signal samples as well as to the samples used to estimate the main prompt SS dilepton backgrounds: WZ, $t\bar{t}W$, $t\bar{t}Z$, $W^\pm W^\pm$. For the WZ and $t\bar{t}Z$ backgrounds, the control region fit results are used for the normalization, so these uncertainties are only applied to the shape of the backgrounds. For the smallest background samples, Rare and $X+\gamma$, a 50% theoretical uncertainty is assigned in place of the scale and PDF variations.

The normalization and the shapes of the nonprompt lepton and charge misidentification backgrounds are estimated from control regions in data. In addition to the statistical uncertainties from the control region yields, dedicated systematic uncertainties are associated with the methods used in this estimate. For the nonprompt lepton background, a 30% uncertainty (increased to 60% for electrons with $p_T > 50\,\text{GeV}$) accounts for the performance of the method in simulation and for the differences in the two alternative methods described in Section 5. In addition, the uncertainty on the prompt-lepton yield in the measurement region, relevant when estimating ϵ_{TL} for high-p_T leptons, results in a 1–30% effect on the estimate. For the charge misidentification background, a 20% uncertainty is assigned to account for possible mismodeling of the charge misidentification rate in simulation.

7   Results and interpretation

A comparison between observed yields and the SM background prediction is shown in Fig. 3 for the kinematic variables used to define the analysis SRs: H_T, E_T^{miss}, m_T^{min}, N_{jets}, and N_b. The distributions are shown after the baseline selection defined in Section 4. The full results of the search in each SR are shown in Fig. 4 and Table 6. The SM predictions are generally consistent with the data. The largest deviations are seen in HL SR 36 and 38, with a local significance, taking these regions individually or combining them with other regions adjacent in phase space, that does not exceed 2 standard deviations.

These results are used to confront the signal models discussed in Section 2: simplified SUSY

Table 5: Summary of the sources of uncertainties and their effect on the yields of different processes in the signal regions. The first two groups list experimental and theoretical uncertainties assigned to processes estimated using simulation, while the last group lists uncertainties assigned to processes whose yield is estimated from data. The uncertainties in the first group also apply to signal samples. Reported values are representative for the most relevant signal regions.

Source	Typical effect (%)
Integrated luminosity	2.6
Lepton selection	4–10
Trigger efficiency	2–7
Pileup	0–6
Jet energy scale	1–15
b tagging	1–15
Monte Carlo stat.	1–10
Scale and PDF variations	10–20
WZ (normalization)	12
$t\bar{t}Z$ (normalization)	30
Nonprompt leptons	30–60
Charge misidentification	20

models, (pseudo)scalar boson production, four top quark production, and SS top quark production. We also interpret the results as model-independent limits as a function of H_T and E_T^{miss}. With the exception of the (pseudo)scalar boson limits at 95% confidence level (CL), the results can be compared to the previous version of the analysis [24], showing significant improvements due to the increase in the integrated luminosity.

To obtain exclusion limits at the 95% confidence, the results from all SRs—including signal and backgrounds uncertainties and their correlations—are combined using an asymptotic formulation of the modified frequentist CL_s criterion [60–63]. When testing a model, all new particles not included in the specific model are considered too heavy to take part in the interaction. To convert cross section limits into mass limits, the signal cross sections specified in Section 2 are used.

The observed SUSY cross section limits as a function of gluino and LSP masses, as well as the observed and expected mass limits for each simplified model, are shown in Fig. 5 for gluino pair production models with each gluino decaying through a chain containing off-shell or on-shell third-generation squarks. These models, which result in two or more b quarks and two or more W bosons in the final state, are introduced in Section 2 as T1tttt, T5ttbbWW, T5tttt, and T5ttcc. Figure 6 shows the limits for a model of gluino production followed by a decay through off-shell first- or second-generation squarks and a chargino. Two different assumptions are made on the chargino mass, taken to be between that of the gluino and the LSP. These T5qqqqWW models result in no b quarks and either on-shell or off-shell W bosons. Bottom squark pair production followed by a decay through a chargino, T6ttWW, resulting in two b quarks and four W bosons, is shown in Fig. 7. For all of the models probed, the observed limit agrees well with the expected one, extending the reach of the previous analysis by 200–300 GeV and reaching 1.5, 1.1, and 0.83 TeV for gluino, LSP, and bottom squark masses, respectively.

The observed and expected cross section limits on the production of a heavy scalar (or pseudoscalar) boson in association to one or two top quarks, followed by its decay to top quarks, are shown in Fig. 8. The limits are compared with the total cross section of the processes described in Section 2, in the scalar and pseudoscalar case. The observed limit, which agrees well with
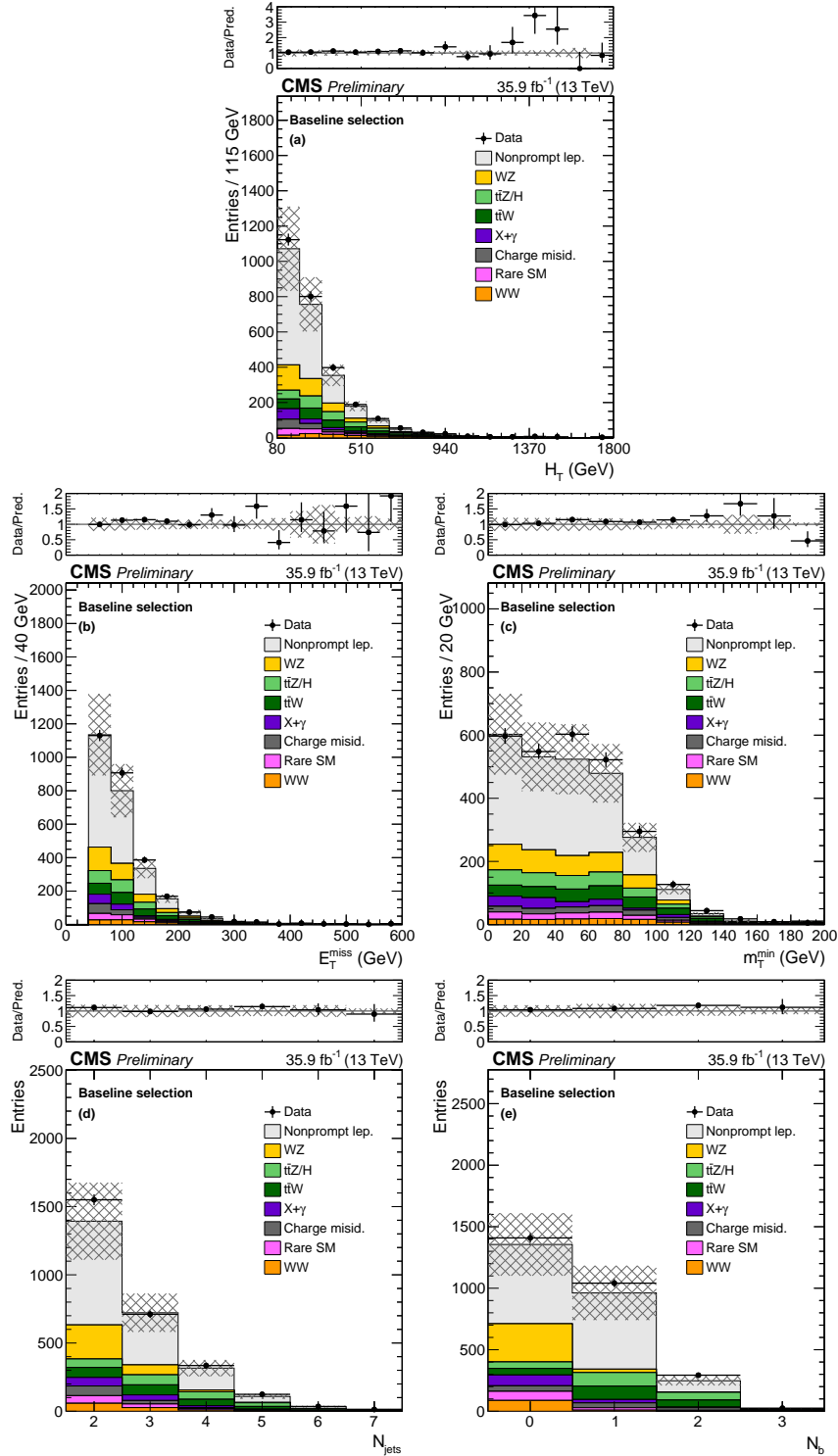
Figure 3: Distributions of the main analysis variables: H_T (a), E_T^{miss} (b), m_T^{min} (c), N_{jets} (d), and N_b (e), after the baseline selection requiring a pair of SS leptons, two jets, and $E_T^{miss} > 50\,\text{GeV}$. The last bin includes the overflow and the hatched area represents the total uncertainty in the background prediction. The upper panels show the ratio of the observed event yield to the background prediction.
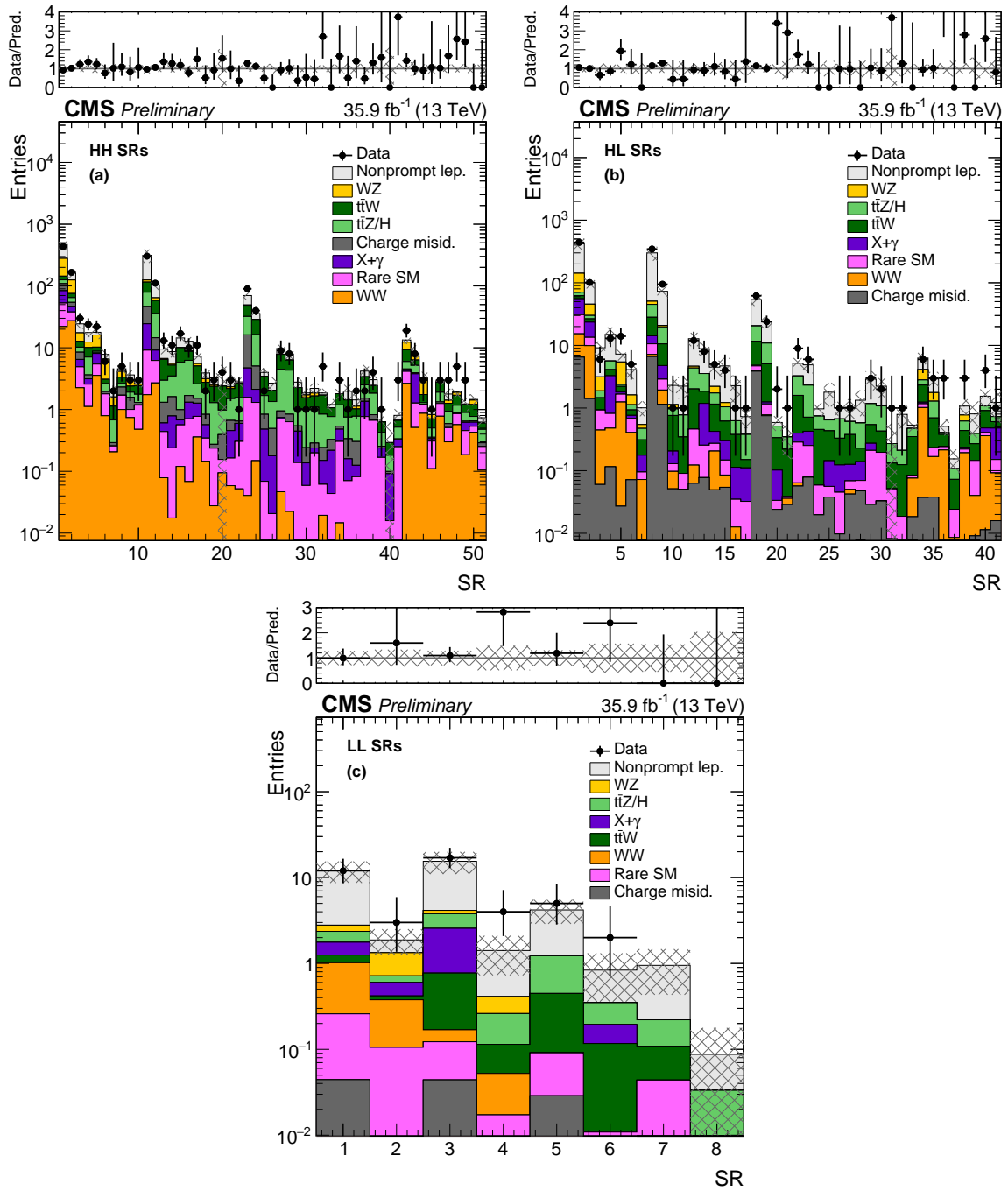
Figure 4: Event yields in the HH (a), HL (b), and LL (c) SRs. The hatched area represents the total uncertainty in the background prediction.

Table 6: Expected number of background and observed events for the different SRs considered in this analysis.

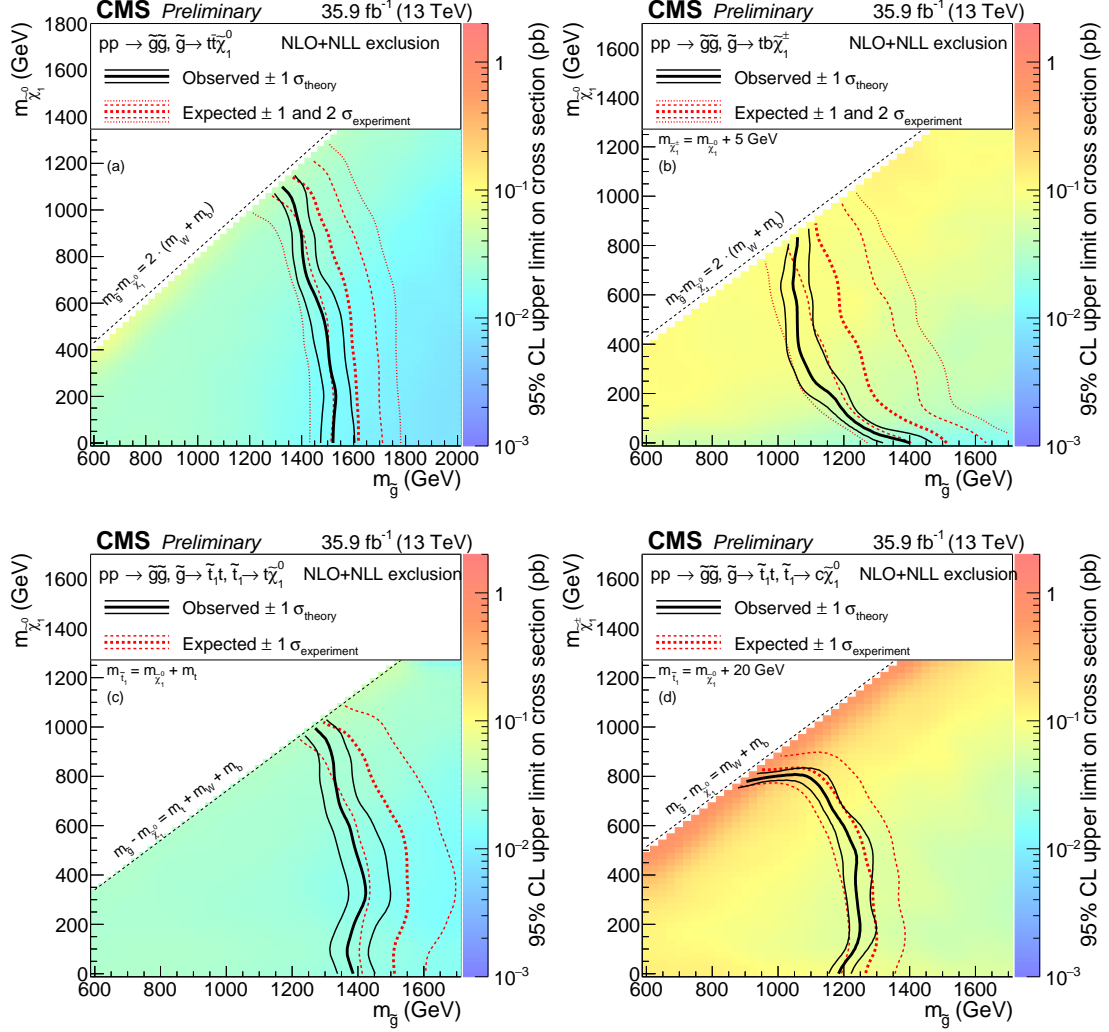|	HH regions		HL regions		LL regions	
	Expected SM	Observed	Expected SM	Observed	Expected SM	Observed
SR1	468.0 ± 98.0	435	419.3 ± 100.0	442	12.0 ± 3.9	12
SR2	161.8 ± 25.1	166	100.4 ± 19.8	101	1.88 ± 0.62	3
SR3	24.4 ± 5.4	30	9.2 ± 2.4	6	15.5 ± 4.7	17
SR4	17.6 ± 3.0	24	15.0 ± 4.5	13	1.42 ± 0.69	4
SR5	17.8 ± 3.9	22	7.3 ± 1.5	14	4.2 ± 1.4	5
SR6	7.8 ± 1.5	6	4.1 ± 1.2	5	0.84 ± 0.48	2
SR7	1.96 ± 0.47	2	1.01 ± 0.28	0	0.95 ± 0.52	0
SR8	4.58 ± 0.81	5	300.3 ± 81.7	346	0.09 ± 0.07	0
SR9	3.63 ± 0.75	3	73.1 ± 17.0	95		
SR10	2.82 ± 0.56	3	2.30 ± 0.61	1		
SR11	313.2 ± 86.8	304	2.24 ± 0.87	1		
SR12	104.0 ± 19.8	111	12.8 ± 3.3	12		
SR13	9.5 ± 1.9	13	8.9 ± 2.3	8		
SR14	8.7 ± 2.0	11	4.5 ± 1.3	5		
SR15	14.4 ± 2.9	17	4.7 ± 1.6	4		
SR16	12.7 ± 2.6	10	2.3 ± 1.1	1		
SR17	7.3 ± 1.2	11	0.73 ± 0.29	1		
SR18	3.92 ± 0.79	2	54.1 ± 12.3	62		
SR19	3.26 ± 0.74	3	23.7 ± 4.9	24		
SR20	2.6 ± 2.7	4	0.59 ± 0.17	2		
SR21	3.02 ± 0.75	3	0.34 ± 0.20	1		
SR22	2.80 ± 0.57	1	5.2 ± 1.2	9		
SR23	70.1 ± 11.9	90	4.9 ± 1.4	6		
SR24	35.7 ± 5.9	40	0.97 ± 0.27	0		
SR25	3.99 ± 0.73	2	1.79 ± 0.74	0		
SR26	2.68 ± 0.80	0	1.01 ± 0.27	1		
SR27	9.7 ± 1.8	9	1.03 ± 0.44	1		
SR28	7.9 ± 2.5	8	1.33 ± 0.61	0		
SR29	2.78 ± 0.58	1	2.89 ± 0.99	3		
SR30	1.86 ± 0.38	1	2.24 ± 0.79	2		
SR31	2.20 ± 0.54	1	0.27 ± 0.30	1		
SR32	1.85 ± 0.39	5	0.79 ± 0.33	1		
SR33	1.20 ± 0.32	0	0.53 ± 0.13	0		
SR34	1.81 ± 0.42	3	6.3 ± 1.3	6		
SR35	1.98 ± 0.61	1	2.92 ± 0.87	3		
SR36	1.43 ± 0.37	2	0.51 ± 0.15	3		
SR37	4.2 ± 1.3	2	0.15 ± 0.07	0		
SR38	3.04 ± 0.68	4	1.07 ± 0.33	3		
SR39	0.63 ± 0.17	1	0.81 ± 0.47	0		
SR40	0.29 ± 0.34	0	1.54 ± 0.50	4		
SR41	0.80 ± 0.22	3	1.23 ± 0.53	1		
SR42	13.4 ± 1.9	19				
SR43	8.0 ± 3.0	8				
SR44	3.33 ± 0.74	3				
SR45	0.94 ± 0.26	1				
SR46	2.92 ± 0.50	3				
SR47	1.78 ± 0.42	3				
SR48	1.95 ± 0.39	5				
SR49	1.23 ± 0.30	3				
SR50	1.46 ± 0.31	0				
SR51	0.74 ± 0.18	0				

Figure 5: Exclusion regions at 95% CL in the $m_{\tilde{\chi}_1^0}$ versus $m_{\tilde{g}}$ plane for the T1tttt (a), T5ttbbWW (b) models with off-shell third generation quarks, and the T5tttt (c) and T5ttcc (d) models, with on-shell third generation quarks. For the T5ttbbWW model, $m_{\tilde{\chi}^\pm} = m_{\tilde{\chi}_1^0} + 5\,\text{GeV}$, for the T5tttt model, $m_{\tilde{t}} - m_{\tilde{\chi}_1^0} = m_t$, and for the T5ttcc model, $m_{\tilde{t}} - m_{\tilde{\chi}_1^0} = 20\,\text{GeV}$ and the decay proceeds through $\tilde{t} \to c\tilde{\chi}_1^0$. The right-hand side color scale indicates the excluded cross section values for a given point in the SUSY particle mass plane. The solid, black curves represent the observed exclusion limits assuming the NLO+NLL cross sections [44–49] (thick line), or their variations of ± 1 standard deviation (thin lines). The dashed, red curves show the expected limits with the corresponding ± 1 and ± 2 standard deviation experimental uncertainties. Excluded regions are to the left and below the limit curves.
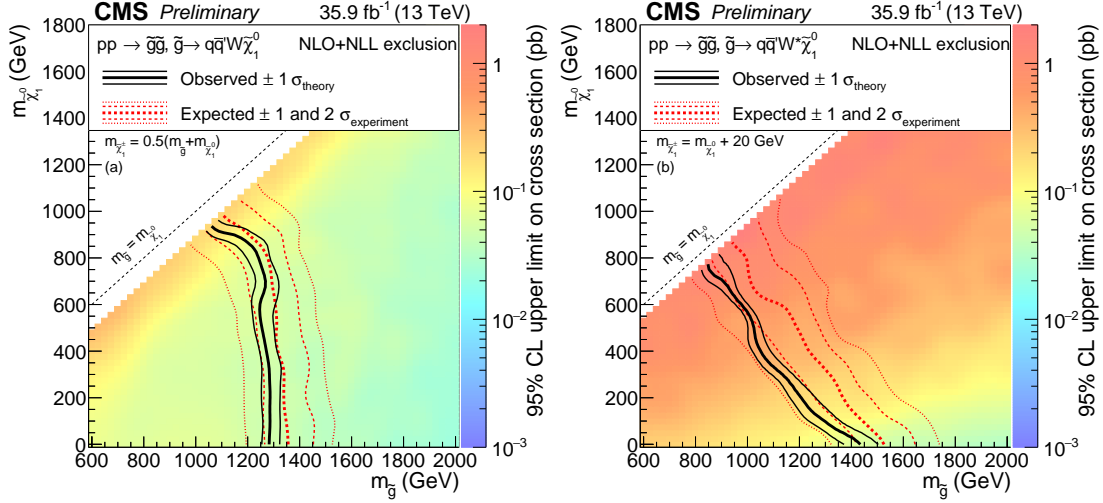
Figure 6: Exclusion regions at 95% CL in the plane of $m_{\tilde{\chi}_1^0}$ versus $m_{\tilde{g}}$ for the T5qqqqWW model with $m_{\tilde{\chi}^\pm} = 0.5(m_{\tilde{g}} + m_{\tilde{\chi}_1^0})$ (a) and with $m_{\tilde{\chi}^\pm} = m_{\tilde{\chi}_1^0} + 20\,\text{GeV}$ (b). For a description of the notation, see Fig. 5.
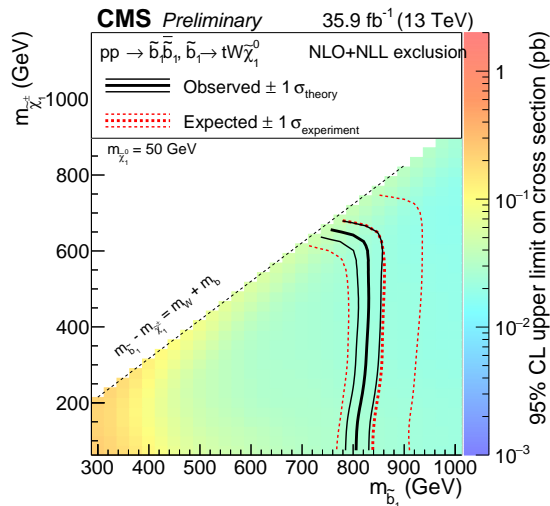

Figure 7: Exclusion regions at 95% CL in the plane of $m_{\tilde{\chi}^\pm}$ versus $m_{\tilde{b}}$ for the T6ttWW model with $m_{\tilde{\chi}_1^0} = 50\,\text{GeV}$. For a description of the notation, see Fig. 5.

the expected one, excludes scalar (pseudoscalar) masses up to 360 (410) GeV.

The SM four top quark production, $\sigma(pp \rightarrow t\bar{t}t\bar{t})$, is normally included among the Rare SM backgrounds. When treating this process as signal, its observed (expected) cross section limit is determined to be 42 fb (27^{+13}_{-8} fb) at 95% CL, to be compared to the SM expectation of 9.1 fb. This is a significant improvement with respect to the observed (expected) limits obtained in the previous version of this analysis, 119 fb (102^{+57}_{-35} fb) [24], and to those obtained in a combination of single-lepton, opposite-sign dilepton, and SS dilepton final states, 69 fb (71^{+38}_{-24} fb) [64]

The results of the search are also used to set a limit on the production cross section for SS top quark pairs, $\sigma(pp \rightarrow tt) + \sigma(pp \rightarrow \bar{t}\bar{t})$. The observed (expected) limit, based on the kinematics of a SM $t\bar{t}$ sample and determined using the number of b jets distribution in the baseline region, is 1.2 pb ($0.76^{+0.3}_{-0.2}$ pb) at 95% CL, significantly improved with respect to the 1.7 pb ($1.5^{+0.7}_{-0.4}$ pb) observed (expected) limit of the previous analysis [24].
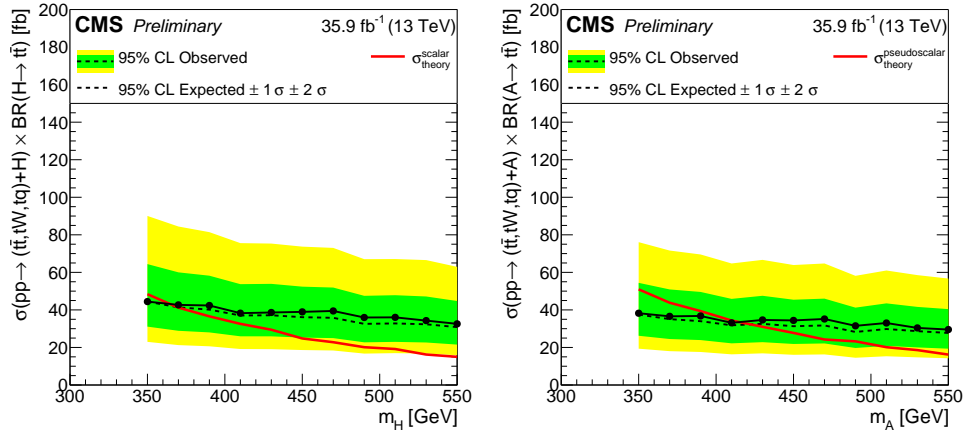

Figure 8: Limits on the production cross section for heavy scalar (left) and pseudoscalar (right) boson in association to one or two top quarks, followed by its decay to top quarks, as a function of the (pseudo)scalar mass. The red line corresponds to the cross section in the (pseudo)scalar model.

7.1   Model-independent limits and additional results

The yields and background predictions can be used to test additional BSM physics scenarios. To facilitate such reinterpretations, limits on the number of SS dilepton pairs as a function of H_T and E_T^{miss} in the kinematic tails are provided, as well as results from a smaller number of inclusive and exclusive signal regions.

The H_T and E_T^{miss} limits are based on combining the tail SRs for the HH selection, respectively 46–51 and 42–45, and employing the CL$_s$ criterion without the asymptotic approximation, as a function of the minimum threshold of each kinematic variable. These limits are presented in Fig. 9 in terms of $\sigma \mathcal{A} \epsilon$, the product of cross section, detector acceptance, and selection efficiency. Where no events are observed, the observed and expected limits reach 0.1 fb, to be compared with the 1.3 fb limit obtained in the previous analysis [24].
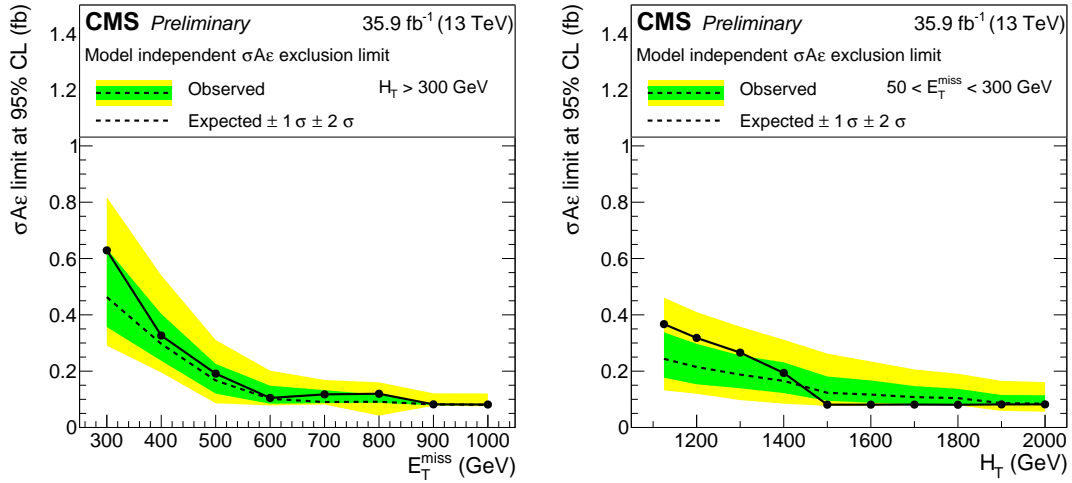

Figure 9: Limits on the product of cross section, detector acceptance, and selection efficiency, $\sigma \mathcal{A} \epsilon$, for the production of an SS dilepton pair as a function of E_T^{miss} (left) and of H_T (right).

Results are also provided in Table 7 for a small number of inclusive signal regions, designed based on different topologies and the requirement of O(5) expected background events. The background expectation, the event count, and the expected BSM yield in any one of these regions can be used to constrain BSM hypotheses in a simple way.

In addition, we define a small number of exclusive signal regions based on integrating over the standard signal regions. Their definitions, as well as the expected and observed yields, are specified in Table 8, while the correlation matrix for the background predictions in these regions is given in Fig. 10. This information can be used to construct a simplified likelihood for models of new physics, as described in Ref. [65].

Table 7: Inclusive SR definitions, expected background yields, and observed yields, as well the observed 95% CL upper limits on the number of signal events contributing to each region. No uncertainty in the signal acceptance is assumed in calculating these limits. A dash in the selections means that the selection is not applied.

SR	Leptons	N_{jets}	N_b	H_T [GeV]	E_T^{miss} [GeV]	m_T^{min} [GeV]	SM expected	Observed	$N_{\text{obs,UL}}^{95\%\text{CL}}$
ISR1		≥ 2	0	≥ 1200	≥ 50	-	4.00 ± 0.79	10	12.35
ISR2		≥ 2	≥ 2	≥ 1100	≥ 50	-	3.63 ± 0.71	4	5.64
ISR3		≥ 2	0	-	≥ 450	-	3.72 ± 0.83	4	5.62
ISR4		≥ 2	≥ 2	-	≥ 300	-	3.32 ± 0.81	6	8.08
ISR5		≥ 2	0	-	≥ 250	≥ 120	1.68 ± 0.44	2	4.46
ISR6	HH	≥ 2	≥ 2	-	≥ 150	≥ 120	3.82 ± 0.76	7	9.06
ISR7		≥ 2	0	≥ 900	≥ 200	-	5.6 ± 1.1	10	10.98
ISR8		≥ 2	≥ 2	≥ 900	≥ 200	-	5.8 ± 1.3	9	9.77
ISR9		≥ 7	-	-	≥ 50	-	10.1 ± 2.7	9	7.39
ISR10		≥ 4	-	-	≥ 50	≥ 120	15.2 ± 3.5	22	16.73
ISR11		≥ 2	≥ 3	-	≥ 50	-	13.3 ± 3.4	17	13.63
ISR12		≥ 2	0	≥ 700	≥ 50	-	3.6 ± 2.5	3	4.91
ISR13	LL	≥ 2	-	-	≥ 200	-	4.9 ± 2.9	10	11.76
ISR14		≥ 5	-	-	≥ 50	-	7.3 ± 5.5	6	6.37
ISR15		≥ 2	≥ 3	-	≥ 50	-	1.06 ± 0.99	0	2.31

Table 8: Exclusive SR definitions, expected background yields, and observed yields.

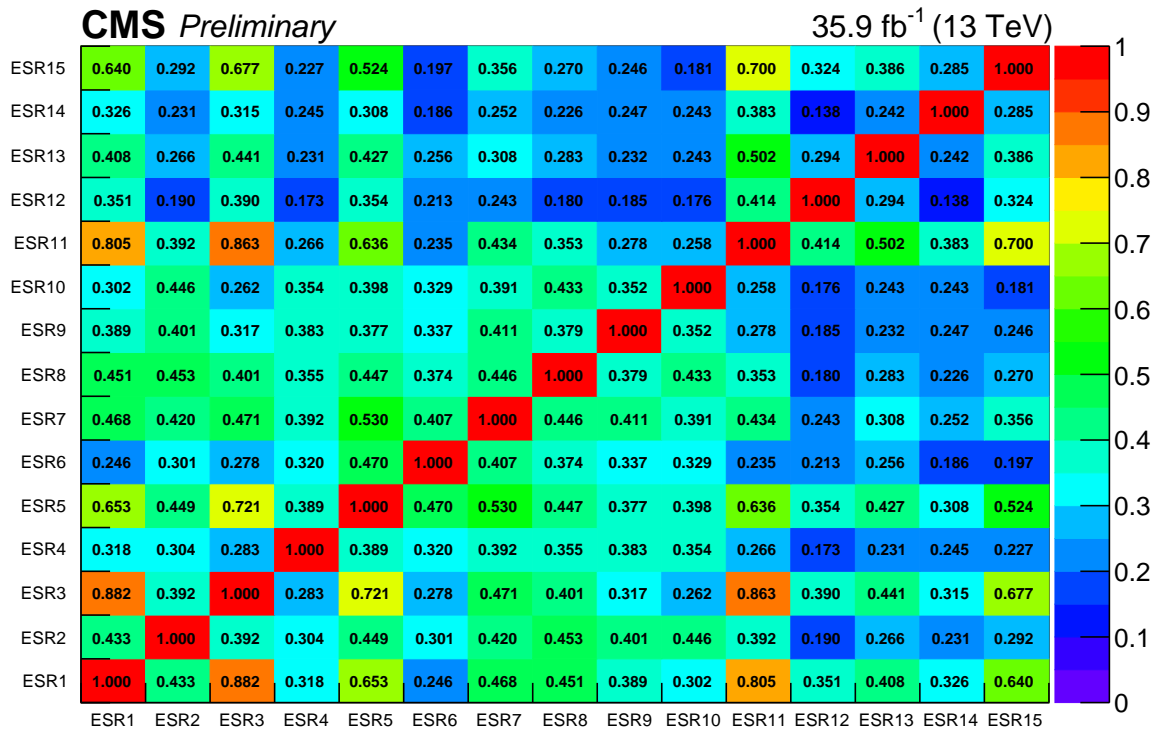| SR	Leptons	N_{jets}	N_b	E_T^{miss} [GeV]	H_T [GeV]	m_T^{min} [GeV]	SM expected	Observed
ESR1		≥ 2	0	50–300	< 1125	< 120 for $H_T > 300$	699.5 ± 130.0	685
ESR2		≥ 2	0	50–300	300–1125	≥ 120	11.0 ± 2.0	11
ESR3		≥ 2	1	50–300	< 1125	< 120 for $H_T > 300$	477.0 ± 120.0	482
ESR4		≥ 2	1	50–300	300–1125	≥ 120	8.4 ± 3.4	8
ESR5		≥ 2	2	50–300	< 1125	< 120 for $H_T > 300$	136.9 ± 23.0	152
ESR6	HH	≥ 2	2	50–300	300–1125	≥ 120	4.9 ± 1.1	8
ESR7		≥ 2	≥ 3	50–300	< 1125	< 120 for $H_T > 300$	11.6 ± 2.9	10
ESR8		≥ 2	≥ 3	50–300	300–1125	≥ 120	0.80 ± 0.22	3
ESR9		≥ 2	-	≥ 300	≥ 300	-	25.7 ± 4.8	31
ESR10		≥ 2	-	50–300	≥ 1125	-	10.1 ± 1.9	14
ESR11		≥ 2	-	50–300	< 1125	< 120	1068.5 ± 250.0	1167
ESR12	HL	≥ 2	-	50–300	< 1125	≥ 120	1.33 ± 0.43	1
ESR13		≥ 2	-	≥ 300	≥ 300	-	9.9 ± 2.3	12
ESR14		≥ 2	-	50–300	≥ 1125	-	4.7 ± 1.7	8
ESR15	LL	≥ 2	-	≥ 50	≥ 300	-	36.9 ± 12.0	43

Figure 10: Correlations between the background predictions in the 15 exclusive regions defined in Section 7.1.

8 Summary

A same-sign dilepton sample corresponding to an integrated luminosity of 35.9 fb^{-1} of proton-proton collisions at 13 TeV has been studied to search for manifestations of BSM physics. The data are found to be consistent with the standard model expectations. The results are interpreted as limits on the cross sections for production of new particles from simplified supersymmetric models. Using calculations for these cross sections as a function of particle mass, these limits have been turned into lower mass limits that are as high 1.5 TeV for gluinos and 0.83 TeV for bottom squarks, depending on the detail of the model. Limits are also provided on the production of heavy scalar and pseudoscalar bosons in the context of two Higgs doublet models, as well as on same-sign top quark pair production, and the standard model production of four top quarks. Finally, to facilitate further interpretations of the search, model-independent limits are provided as a function of H_{T} and $E_{\mathrm{T}}^{\mathrm{miss}}$, together with the background prediction and data yields in a smaller set of signal regions.

References

[1] R. M. Barnett, J. F. Gunion, and H. E. Haber, "Discovering supersymmetry with like-sign dileptons", *Phys. Lett. B* **315** (1993) 349, `doi:10.1016/0370-2693(93)91623-U`, `arXiv:hep-ph/9306204`.

[2] M. Guchait and D. P. Roy, "Like-sign dilepton signature for gluino production at CERN LHC including top quark and Higgs boson effects", *Phys. Rev. D* **52** (1995) 133, `doi:10.1103/PhysRevD.52.133`, `arXiv:hep-ph/9412329`.

[3] Y. Bai and Z. Han, "Top-antitop and top-top resonances in the dilepton channel at the CERN LHC", *JHEP* **04** (2009) 056, `doi:10.1088/1126-6708/2009/04/056`, `arXiv:0809.4487`.

[4] E. L. Berger et al., "Top quark forward-backward asymmetry and same-sign top quark pairs", *Phys. Rev. Lett.* **106** (2011) 201801, `doi:10.1103/PhysRevLett.106.201801`, `arXiv:1101.5625`.

[5] T. Plehn and T. M. P. Tait, "Seeking Sgluons", *J. Phys. G* **36** (2009) 075001, `doi:10.1088/0954-3899/36/7/075001`, `arXiv:0810.3919`.

[6] S. Calvet, B. Fuks, P. Gris, and L. Valery, "Searching for sgluons in multitop events at a center-of-mass energy of 8 TeV", *JHEP* **04** (2013) 043, `doi:10.1007/JHEP04(2013)043`, `arXiv:1212.3360`.

[7] K. J. F. Gaemers and F. Hoogeveen, "Higgs Production and Decay Into Heavy Flavors With the Gluon Fusion Mechanism", *Phys. Lett. B* **146** (1984) 347, `doi:10.1016/0370-2693(84)91711-8`.

[8] G. C. Branco et al., "Theory and phenomenology of two-Higgs-doublet models", *Phys. Rept.* **516** (2012) 1, `doi:10.1016/j.physrep.2012.02.002`, `arXiv:1106.0034`.

[9] F. M. L. Almeida, Jr. et al., "Same-sign dileptons as a signature for heavy Majorana neutrinos in hadron-hadron collisions", *Phys. Lett. B* **400** (1997) 331, `doi:10.1016/S0370-2693(97)00143-3`, `arXiv:hep-ph/9703441`.

[10] R. Contino and G. Servant, "Discovering the top partners at the LHC using same-sign dilepton final states", *JHEP* **06** (2008) 026, `doi:10.1088/1126-6708/2008/06/026`, `arXiv:0801.1679`.

[11] P. Ramond, "Dual theory for free fermions", *Phys. Rev. D* **3** (1971) 2415, `doi:10.1103/PhysRevD.3.2415`.

[12] Y. A. Gol'fand and E. P. Likhtman, "Extension of the algebra of Poincaré group generators and violation of P invariance", *JETP Lett.* **13** (1971) 323.

[13] A. Neveu and J. H. Schwarz, "Factorizable dual model of pions", *Nucl. Phys. B* **31** (1971) 86, `doi:10.1016/0550-3213(71)90448-2`.

[14] D. V. Volkov and V. P. Akulov, "Possible universal neutrino interaction", *JETP Lett.* **16** (1972) 438.

[15] J. Wess and B. Zumino, "A lagrangian model invariant under supergauge transformations", *Phys. Lett. B* **49** (1974) 52, `doi:10.1016/0370-2693(74)90578-4`.

[16] J. Wess and B. Zumino, "Supergauge transformations in four-dimensions", *Nucl. Phys. B* **70** (1974) 39, `doi:10.1016/0550-3213(74)90355-1`.

[17] P. Fayet, "Supergauge invariant extension of the Higgs mechanism and a model for the electron and its neutrino", *Nucl. Phys. B* **90** (1975) 104, `doi:10.1016/0550-3213(75)90636-7`.

[18] H. P. Nilles, "Supersymmetry, supergravity and particle physics", *Phys. Rept.* **110** (1984) 1, `doi:10.1016/0370-1573(84)90008-5`.

[19] S. P. Martin, "A supersymmetry primer", in *Perspectives on Supersymmetry II*, G. L. Kane, ed., p. 1. World Scientific, 2010. `arXiv:hep-ph/9709356`. Adv. Ser. Direct. High Energy Phys., vol. 21. `doi:10.1142/9789814307505_0001`.

[20] P. Fayet, "About R-parity and the supersymmetric standard model", `doi:10.1142/9789812793850_0027`, `arXiv:hep-ph/9912413`.

[21] D. Dicus, A. Stange, and S. Willenbrock, "Higgs decay to top quarks at hadron colliders", *Phys. Lett. B* **333** (1994) 126, `doi:10.1016/0370-2693(94)91017-0`, `arXiv:hep-ph/9404359`.

[22] N. Craig et al., "The Hunt for the Rest of the Higgs Bosons", *JHEP* **06** (2015) 137, `doi:10.1007/JHEP06(2015)137`, `arXiv:1504.04630`.

[23] N. Craig et al., "Heavy Higgs bosons at low $\tan\beta$: from the LHC to 100 TeV", *JHEP* **01** (2017) 018, `doi:10.1007/JHEP01(2017)018`, `arXiv:1605.08744`.

[24] CMS Collaboration, "Search for new physics in same-sign dilepton events in proton-proton collisions at $\sqrt{s} = 13$ TeV", *Eur. Phys. J. C* **76** (2016) 439, `doi:10.1140/epjc/s10052-016-4261-z`, `arXiv:1605.03171`.

[25] ATLAS Collaboration, "Search for gluinos in events with two same-sign leptons, jets and missing transverse momentum with the ATLAS detector in pp collisions at $\sqrt{s} = 7$ TeV", *Phys. Rev. Lett.* **108** (2012) 241802, `doi:10.1103/PhysRevLett.108.241802`, `arXiv:1203.5763`.

[26] ATLAS Collaboration, "Search for supersymmetry at $\sqrt{s} = 8$ TeV in final states with jets and two same-sign leptons or three leptons with the ATLAS detector", *JHEP* **06** (2014) 035, `doi:10.1007/JHEP06(2014)035`, `arXiv:1404.2500`.

[27] ATLAS Collaboration, "Search for supersymmetry at $\sqrt{s} = 13$ TeV in final states with jets and two same-sign leptons or three leptons with the ATLAS detector", *Eur. Phys. J. C* **76** (2016) 259, `doi:10.1140/epjc/s10052-016-4095-8`, `arXiv:1602.09058`.

[28] CMS Collaboration, "Search for new physics with same-sign isolated dilepton events with jets and missing transverse energy at the LHC", *JHEP* **06** (2011) 077, `doi:10.1007/JHEP06(2011)077`, `arXiv:1104.3168`.

[29] CMS Collaboration, "Search for new physics in events with same-sign dileptons and b-tagged jets in pp collisions at $\sqrt{s} = 7$ TeV", *JHEP* **08** (2012) 110, `doi:10.1007/JHEP08(2012)110`, `arXiv:1205.3933`.

[30] CMS Collaboration, "Search for new physics with same-sign isolated dilepton events with jets and missing transverse energy", *Phys. Rev. Lett.* **109** (2012) 071803, `doi:10.1103/PhysRevLett.109.071803`, `arXiv:1205.6615`.

[31] CMS Collaboration, "Search for new physics in events with same-sign dileptons and b jets in pp collisions at $\sqrt{s} = 8$ TeV", *JHEP* **03** (2013) 037, `doi:10.1007/JHEP03(2013)037,10.1007/JHEP07(2013)041`, `arXiv:1212.6194`. [Erratum: *JHEP* **07** (3013) 041].

[32] CMS Collaboration, "Search for new physics in events with same-sign dileptons and jets in pp collisions at 8 TeV", *JHEP* **01** (2014) 163, `doi:10.1007/JHEP01(2014)163`, `arXiv:1311.6736`.

[33] J. Alwall et al., "The automated computation of tree-level and next-to-leading order differential cross sections, and their matching to parton shower simulations", *JHEP* **07** (2014) 079, `doi:10.1007/JHEP07(2014)079`, `arXiv:1405.0301`.

[34] T. Melia, P. Nason, R. Rontsch, and G. Zanderighi, "W^+W^-, WZ and ZZ production in the POWHEG BOX", *JHEP* **11** (2011) 078, `doi:10.1007/JHEP11(2011)078`, `arXiv:1107.5051`.

[35] P. Nason and G. Zanderighi, "W^+W^- , WZ and ZZ production in the POWHEG BOX V2", *Eur. Phys. J. C* **74** (2014) 2702, `doi:10.1140/epjc/s10052-013-2702-5`, `arXiv:1311.1365`.

[36] NNPDF Collaboration, "Parton distributions for the LHC Run II", *JHEP* **04** (2015) 040, `doi:10.1007/JHEP04(2015)040`, `arXiv:1410.8849`.

[37] T. Sjostrand, S. Mrenna, and P. Z. Skands, "A Brief Introduction to PYTHIA 8.1", *Comput. Phys. Commun.* **178** (2008) 852, `doi:10.1016/j.cpc.2008.01.036`, `arXiv:0710.3820`.

[38] P. Skands, S. Carrazza, and J. Rojo, "Tuning PYTHIA 8.1: the Monash 2013 tune", *Eur. Phys. J. C* **74** (2014) 3024, `doi:10.1140/epjc/s10052-014-3024-y`, `arXiv:1404.5630`.

[39] CMS Collaboration, "Event generator tunes obtained from underlying event and multiparton scattering measurements", *Eur. Phys. J. C* **76** (2016) 155, `doi:10.1140/epjc/s10052-016-3988-x`, `arXiv:1512.00815`.

[40] GEANT4 Collaboration, "GEANT4—a simulation toolkit", *Nucl. Instrum. Meth. A* **506** (2003) 250, `doi:10.1016/S0168-9002(03)01368-8`.

[41] S. Abdullin et al., "The fast simulation of the CMS detector at LHC", *J. Phys. Conf. Ser.* **331** (2011) 032049, `doi:10.1088/1742-6596/331/3/032049`.

[42] D. Alves et al., "Simplified models for LHC new physics searches", *J. Phys. G* **39** (2012) 105005, `doi:10.1088/0954-3899/39/10/105005`, `arXiv:1105.2838`.

[43] CMS Collaboration, "Interpretation of searches for supersymmetry with simplified models", *Phys. Rev. D* **88** (2013) 052017, `doi:10.1103/PhysRevD.88.052017`, `arXiv:1301.2175`.

[44] W. Beenakker, R. Höpker, M. Spira, and P. M. Zerwas, "Squark and gluino production at hadron colliders", *Nucl. Phys. B* **492** (1997) 51, `doi:10.1016/S0550-3213(97)80027-2`, `arXiv:hep-ph/9610490`.

[45] A. Kulesza and L. Motyka, "Threshold resummation for squark-antisquark and gluino-pair production at the LHC", *Phys. Rev. Lett.* **102** (2009) 111802, `doi:10.1103/PhysRevLett.102.111802`, `arXiv:0807.2405`.

[46] A. Kulesza and L. Motyka, "Soft gluon resummation for the production of gluino-gluino and squark-antisquark pairs at the LHC", *Phys. Rev. D* **80** (2009) 095004, `doi:10.1103/PhysRevD.80.095004`, `arXiv:0905.4749`.

[47] W. Beenakker et al., "Soft-gluon resummation for squark and gluino hadroproduction", *JHEP* **12** (2009) 041, `doi:10.1088/1126-6708/2009/12/041`, `arXiv:0909.4418`.

[48] W. Beenakker et al., "Squark and gluino hadroproduction", *Int. J. Mod. Phys. A* **26** (2011) 2637, `doi:10.1142/S0217751X11053560`, `arXiv:1105.1110`.

[49] C. Borschensky et al., "Squark and gluino production cross sections in pp collisions at $\sqrt{s}$ = 13, 14, 33 and 100 TeV", *Eur. Phys. J. C* **74** (2014) 3174, `doi:10.1140/epjc/s10052-014-3174-y`, `arXiv:1407.5066`.

[50] CMS Collaboration, "The CMS experiment at the CERN LHC", *JINST* **3** (2008) S08004, `doi:10.1088/1748-0221/3/08/S08004`.

[51] CMS Collaboration, "The CMS trigger system", *JINST* **12** (2017) P01020, `doi:10.1088/1748-0221/12/01/P01020`, `arXiv:1609.02366`.

[52] CMS Collaboration, "Particle-flow event reconstruction in CMS and performance for jets, taus, and $E_\mathrm{T}^\mathrm{miss}$", CMS Physics Analysis Summary CMS-PAS-PFT-09-001, CERN, 2009.

[53] CMS Collaboration, "Commissioning of the particle-flow event reconstruction with the first LHC collisions recorded in the CMS detector", CMS Physics Analysis Summary CMS-PAS-PFT-10-001, CERN, 2010.

[54] M. Cacciari, G. P. Salam, and G. Soyez, "The anti-k_t jet clustering algorithm", *JHEP* **04** (2008) 063, `doi:10.1088/1126-6708/2008/04/063`, `arXiv:0802.1189`.

[55] M. Cacciari, G. P. Salam, and G. Soyez, "FastJet user manual", *Eur. Phys. J. C* **72** (2012) 1896, `doi:10.1140/epjc/s10052-012-1896-2`, `arXiv:1111.6097`.

[56] CMS Collaboration, "Determination of jet energy calibration and transverse momentum resolution in CMS", *JINST* **6** (2011) P11002, `doi:10.1088/1748-0221/6/11/P11002`, `arXiv:1107.4277`.

[57] CMS Collaboration, "Jet energy scale and resolution in the CMS experiment in pp collisions at 8 TeV", *JINST* **12** (2016) P02014, `doi:10.1088/1748-0221/12/02/P02014`, `arXiv:1607.03663`.

[58] CMS Collaboration, "Performance of the CMS missing transverse momentum reconstruction in pp data at $\sqrt{s}$ = 8 TeV", *JINST* **10** (2015) P02006, `doi:10.1088/1748-0221/10/02/P02006`, `arXiv:1411.0511`.

[59] ATLAS Collaboration, "Search for anomalous production of prompt same-sign lepton pairs and pair-produced doubly charged Higgs bosons with $\sqrt{s} = 8$ TeV *pp* collisions using the ATLAS detector", *JHEP* **03** (2015) 041, `doi:10.1007/JHEP03(2015)041`, `arXiv:1412.0237`.

[60] T. Junk, "Confidence level computation for combining searches with small statistics", *Nucl. Instrum. Meth. A* **434** (1999) 435, `doi:10.1016/S0168-9002(99)00498-2`, `arXiv:hep-ex/9902006`.

[61] A. L. Read, "Presentation of search results: The CL$_S$ technique", *J. Phys. G* **28** (2002) 2693, `doi:10.1088/0954-3899/28/10/313`.

[62] ATLAS and CMS Collaborations, "Procedure for the LHC Higgs boson search combination in summer 2011", ATL-PHYS-PUB-2011-011, CMS NOTE-2011/005, 2011.

[63] G. Cowan, K. Cranmer, E. Gross, and O. Vitells, "Asymptotic formulae for likelihood-based tests of new physics", *Eur. Phys. J. C* **71** (2011) 1554, `doi:10.1140/epjc/s10052-011-1554-0,10.1140/epjc/s10052-013-2501-z`, `arXiv:1007.1727`. [Erratum: *Eur. Phys. J. C* **73** (2013) 2501].

[64] CMS Collaboration, "Search for standard model production of four top quarks in proton-proton collisions at $\sqrt{s}$ = 13 TeV", `arXiv:1702.06164`.

[65] CMS Collaboration, "Simplified likelihood for the re-interpretation of public CMS results", Technical Report CERN-CMS-NOTE-2017-001, CERN, Geneva, Jan, 2017.